Ir(III) Diamine Transfer Hydrogenation Catalysts in Cancer Cells

Fry, Millie E.; Alsaif, Sitah; Khanom, Yasmin; Keirle, Alice K.; Pheasey, Chloe E.; Song, Ji Inn; Bedford, Rebecca A.; Romero Canelon, Isolda; Sadler, Peter J; Coverdale, James

DOI:
10.1002/cctc.202401490

Research Article
doi.org/10.1002/cctc.202401490
Chemistry Europe
European Chemical Societies Publishing

www.chemcatchem.org

Ir(III) Diamine Transfer Hydrogenation Catalysts in Cancer Cells

Millie E. Fry,[a] Sitah A. Alsaif,[a] Yasmin Khanom,[b] Alice K. Keirle,[a] Chloe E. Pheasey,[a] Ji Inn Song,[b] Rebecca A. Bedford,[a] Isolda Romero-Canelon,[a, b] Peter J. Sadler,[b] and James P. C. Coverdale*[a, b]

The development of catalytic metallodrugs is an emerging field that may offer new approaches to cancer chemotherapeutic design. By exploiting the unique properties of transition metal complexes, in-cell catalysis can be applied to modulate the cellular redox balance as part of a multi-targeting mechanism of action. We describe the synthesis and characterization of six coordinatively unsaturated iridium(III) diamine catalysts that are stable at physiological pH in aqueous solution. Reduction of the colorimetric substrate 2,6-dichlorophenolindophenol by transfer hydrogenation under biologically compatible conditions achieved turnover frequencies up to 63 ± 2 h^{-1} and demonstrated that the source of hydride (sodium formate) is the limiting reagent, despite being in a 1000-fold excess of the catalyst. The catalyst showed low in vivo acute toxicity in zebrafish embryos and modest in vitro potency towards cancer cells. When administered alone, the catalyst generated oxidative stress in cells (an effect that was conserved in vivo), but co-treatment with a nontoxic dose of sodium formate negated this effect. Co-treatment with sodium formate significantly enhanced catalyst potency in cancer cells (A2780 ovarian and MCF7 breast cancer cells) and drug-resistant cells (A2780cis and MCF7-TAMR1) but not in non-tumorigenic cells (MRC5), demonstrating that a redox-targeting mechanism may generate selectivity for cancer cells.

1. Introduction

Modulation of cellular redox using an in-cell catalyst exploits an inherent vulnerability of cancer cells.[1] Redox disruption is a multi-targeting approach which impacts various cellular processes,[2] as opposed to targeted therapeutics, for which resistance mechanisms may readily develop.[3] Various examples of subcellular redox perturbation have been described, including nicotinamide adenine dinucleotide (NAD^+/NADH),[4] pyruvate/lactate,[4e,5] quinone/hydroquinone,[6] and glutathione (GSH/GSSG).[7] Second and third row transition metal ions offer the kinetic inertness required to deliver an intact catalyst to a biological system rich in nucleophiles (e.g., thiols) which would otherwise poison or deactivate the catalyst. While cyclometalated catalysts and protein scaffold artificial metalloenzymes have shown promise,[4h,8] metal-arene *N*-tosyldiamine catalysts have proven particularly attractive for in-cell applications, since the chemistry of the catalyst cycle is well defined.[9] A 50-fold increase in the potency of a Ru(II) *N*-tosyldiamine catalyst was achieved in A2780 ovarian cancer cells by coadministration with sodium formate (a sacrificial source of reducing hydride). This therapeutic combination was not only synergistic but demonstrated the first example of in-cell catalytic reduction, converting the coenzyme NAD^+ to NADH.[4a] It was since shown that catalytic performance is highly dependent on both steric and electronic effects at the *N*-substituent.[4b] Using a chiral Os(II) diamine catalyst, we reported the first example of in-cell asymmetric transfer hydrogenation, catalytically generating unnatural D-lactate from endogenous pyruvate with high enantioselectivity.[5a] With this system, we demonstrated the potential of using catalytic metallodrugs to overcome drug resistance in cisplatin- and tamoxifen-resistant cells, while no significant catalytic potency modulation was observed in non-cancerous cells.[5b,10] More recently, we have shown that the catalytic generation of lactate can be enhanced as part of a combination therapy involving a metal catalyst and a monocarboxylate transporter inhibitor,[5b] and have described structural improvements to the catalyst involving covalent tethering of the diamine to the η^6-arene ligand.[11]

Inspired by biocompatible Ru(II) and Os(II) catalyst systems, interests have expanded to include Ir(III) catalysts. Iridium(III) picolinate catalysts have been shown to catalyze NADH oxidation and increase levels of reactive oxygen species (ROS) in cancer cells,[12] while iridium(III) 2,2′-bipyridine catalysts have been shown to catalyze the photooxidation of the coenzyme NADPH, with examples achieving turnover frequencies up to 308.0 h^{-1}.[13] While the Ir(III) *N*-tosyldiamine catalyst [IrCl(Cp*)(TsDPEN-H)] is well established for conventional chemical catalysis,[14] it has not been explored within the context of medicinal chemistry. In this work, we report a new family

[a] M. E. Fry, S. A. Alsaif, A. K. Keirle, C. E. Pheasey, R. A. Bedford, I. Romero-Canelon, J. P. C. Coverdale
School of Pharmacy, School of Health Sciences, College of Medicine and Health, University of Birmingham, Edgbaston B15 2TT, UK
E-mail: j.p.coverdale@bham.ac.uk

[b] Y. Khanom, J. I. Song, I. Romero-Canelon, P. J. Sadler, J. P. C. Coverdale
Department of Chemistry, University of Warwick, Coventry CV4 7AL, UK

Supporting information for this article is available on the WWW under https://doi.org/10.1002/10.1002/cctc.202401490

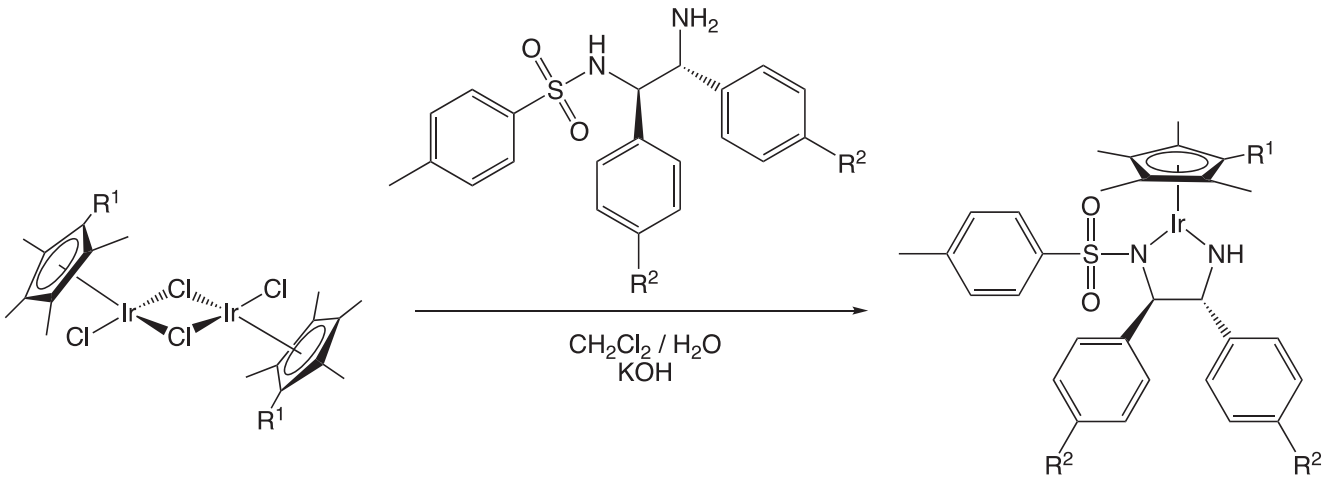

Figure 1. Synthesis of Ir catalysts **1**–**6** studied in this work. Ir catalysts **1**–**3** bear the TsDPEN (*N*-tosyl diphenyl ethylenediamine) bidentate ligand, while Ir catalysts **4**–**6** introduce a methoxy (R_2 = OCH_3) substituent on the chiral diamine ligand to improve aqueous solubility.

Table 1. Physicochemical, in vitro, and in vivo biological properties of Ir complexes 1–**6** and cisplatin. Hydrophobicities determined experimentally as octanol/water partition coefficients (Log PO/W) by ICP-MS in experimental triplicate. Antiproliferative activities (IC50/μM, 24 h exposure + 72 h recovery time, sulforhodamine B assay, duplicate of triplicate analysis). Cellular Ir accumulation (fg Ir cell-1, 1 × IC50 concentration, 24 h, no recovery time) determined using A2780 cancer cells (independent triplicate experiments, N = 3). In vivo toxicities (LC50/μM, 96 h exposure) determined in Singapore wild-type zebrafish embryos (*Danio rerio*) as described by OECD test 236: acute zebrafish embryo toxicity test (two independent duplicate experiments). N.D. = not determined.

	R1	R2	Log PO/W	A2780 IC50/μM	A2780 Ir/fg·cell^{-1}	*Danio rerio* LC50/μM
1	CH3	H	0.86 ± 0.02	20.9 ± 0.7	52 ± 1	8 ± 1
2	Phenyl	H	1.41 ± 0.02	14 ± 2	41.7 ± 0.7	1.6 ± 0.3
3	Biphenyl	H	2.24 ± 0.02	10.2 ± 0.6	89 ± 4	0.7 ± 0.1
4	CH3	OCH3	0.03 ± 0.04	17 ± 1	8 ± 1	11 ± 2
5	Phenyl	OCH3	0.32 ± 0.02	8.0 ± 0.8	13 ± 1	3.6 ± 0.2
6	Biphenyl	OCH3	0.62 ± 0.03	0.7 ± 0.1	5.3 ± 0.2	2.9 ± 0.8
Cisplatin	N/A	N/A	N.D.	1.2 ± 0.3	N/A	0.6 ± 0.2

of coordinatively unsaturated 16-electron organo-Ir(III) catalysts and have investigated their mechanism of action and ability to catalyze transfer hydrogenation reactions inside cells.

2. Results and Discussion

Iridium catalyst **1** [Ir(Cp*)(TsDPEN)] is derived from 18-electron chlorido pre-catalyst [IrCl(Cp*)(TsDPEN-H)], which has previously been shown to achieve the rapid conversion of ketones to chiral alcohols with high enantioselectivity in an organic solvent system within the context of synthetic chemistry.[14] Catalyst **1** is the active catalytic species, which can be readily prepared by treatment of the pre-catalyst with a suitable base to eliminate HCl. Alternatively, catalyst **1** may be prepared in a one-pot reaction from a precursor Ir(III) cyclopentadienyl (Cp*) dimer, *N*-tosyl diphenyl ethylenediamine (TsDPEN), and a base, utilizing a biphasic reaction optimized for the preparation of structurally similar Os(II) catalysts (Figure 1, Table 1).[15] Like its osmium(II) counterpart,[5a] this 16-electron Ir(III) catalyst is highly stable in air and solution. Time-dependent ^{1}H-NMR spectra acquired in deuterated dimethyl sulfoxide did not exhibit any new or shifted peaks after 24 h compared to the initial (t = 0 h) spectrum (Supporting Information Figure S1). Similarly, UV–vis spectroscopic measurements showed catalyst **1** to be stable in phosphate-buffered saline (containing 10% v/v dimethyl sulfoxide to aid solubility) for 24 h (Supporting Information Figure S2). Though it is possible that modification, ligand substitution, or degradation may occur on a timescale more rapid than the experimental design, the chemical species identified in the first spectrum acquired (ca. 10 min) remained unchanged for the 24 h period investigated and did not undergo further structural modifications.

Extended arene catalysts **2** (Cp^{xPh}) and **3** (Cp^{xBip}) were prepared in a similar manner to catalyst **1**, using extended arene dimer precursors (R^1 = phenyl or biphenyl, for **2** and **3**, respectively) and were obtained as purple amorphous solids, which were recrystallized from dichloromethane/hexane. To improve aqueous solubility, methoxyphenyl-functionalized catalysts **4**–**6** (R^2 = OCH_3) were prepared with equivalent arene ligands (Cp*, Cp^{xPh}, and Cp^{xBip}). This structural modification significantly increased the hydrophilicity of catalysts **4**–**6** (Log $P_{O/W}$ = 0.03,

0.32, and 0.62, respectively) in comparison to their unfunctionalized analogues **1–3** (Log $P_{O/W}$ = 0.86, 1.41, and 2.24, respectively).

An ideal in-cell transfer hydrogenation (reduction) catalyst should not be significantly toxic when administered alone to ensure that a significant intracellular concentration can be achieved prior to initiating catalysis by coadministration of a source of reducing hydride. The zebrafish embryo (*Danio rerio*) model was used to assess acute toxicity, and its suitability to support small molecule therapeutic development has been extensively reviewed.[16] Remarkably, catalyst **1** (LC_{50} = 8 ± 1 μM) was threefold less toxic than its isoelectronic Os(II) analogue [Os(*p*-cymene)(TsDPEN)] (LC_{50} = 2.4 ± 0.4 μM) and over an order of magnitude less toxic than cisplatin (LC_{50} = 0.6 ± 0.2 μM) and structurally similar Ir(III) azopyridine piano-stool catalysts.[10,17] While methoxyphenyl-functionalization did not significantly impact acute toxicity, toxicity increased with increasing arene extension ($Cp^* < Cp^{xPh} < Cp^{xBip}$, Figure 1, Table 1).

With encouraging in vivo data to support the further study of this catalyst system in living cells, antiproliferative activities were determined using A2780 ovarian cancer cells. Methoxyphenyl-functionalized catalysts **4–6** were more potent than **1–3**, and the anticancer activity of catalyst **6** exceeded that of cisplatin (catalyst **6** IC_{50} = 0.7 ± 0.1 μM, cisplatin IC_{50} = 1.2 ± 0.3 μM). Within each series of compounds containing the same bidentate ligand (**1–3** and **4–6**), IC_{50} values directly correlated with lipophilicity (Log P, Figure 1, Table 1). However, ICP-MS analysis of cells treated with equipotent concentrations of Ir catalyst revealed that intracellular accumulation of Ir in cells treated with **1–3** was an order of magnitude greater (41.7–89 fg Ir·cell^{-1}) than those treated with equipotent concentrations of **4–6** (5.3–13 fg Ir·cell^{-1}). Therefore, although methoxy-functionalized catalysts **4–6** achieved high potency at low intracellular Ir accumulation, in this work we aimed to achieve in-cell catalysis, and improving catalyst in-cell availability was a critical objective.

Catalysts **1–3** were subsequently screened for activity towards 13 human cell lines (Table 2). Increased potency is correlated with arene extension ($Cp^* < Cp^{xPh} < Cp^{xBip}$) with some examples exceeding the anticancer activity of cisplatin. A direct correlation was observed between potency (IC_{50}) and Ir cellular accumulation, leading us to focus on ovarian (A2780) and breast (MCF7) cells, in which Ir accumulation was greatest. Activities were not significantly different between A2780 (cisplatin-sensitive ovarian cancer cells) and A2780cis (cisplatin-resistant ovarian cancer cells), suggesting that Ir(III) catalysts **1–3** do not share a common mechanism of resistance with cisplatin in this cell line. Overcoming cisplatin resistance is frequently observed for Ir piano-stool catalysts, including those bearing azopyridine and iminopyridine ligands,[17,18] as well as alcohol-functionalized Ir Cp* dimeric catalysts.[19] Antiproliferative activities determined in HCT116 colorectal cancer cells with either p53 knockout or p21 knockout were higher (less potent) than those determined in the parental HCT116 cell line, which might implicate p53 or p21 proteins in the mechanism of action of **1**. While no significant cell cycle arrest was observed in A2780 cells treated with sodium formate relative to the untreated control (Figure 2a and Supporting Information), a small increase in G_2/M arrest was observed in the presence of catalyst **1**, irrespective of formate co-treatment (G_2/M population increased from 12.0 ± 0.5% in the untreated control to 15.4 ± 0.8% in the presence of **1**). Nonetheless, this increase was far less prominent than the S and G_2/M-phase arrest (S phase = 37 ± 1%, G_2/M-phase = 35.4 ± 0.2%) observed upon cisplatin treatment ($P < 0.001$).

Subcellular fractionation of A2780 cancer cells treated with catalyst **1** revealed Ir to be predominantly located in the membrane/organelle fraction (61 ± 2%) and only a small percentage of Ir located in the nucleic fraction (1.2 ± 0.6%). This result is comparable to studies using the osmium(II) *p*-cymene analogue of catalyst **1** (membrane/organelle fraction: 48 ± 3%, nucleic fraction: 1.6 ± 0.5%) but contrasts with A2780 cells treated with cisplatin, where 4.9 ± 0.8% of the total cellular Pt was found in the nucleic fraction (Figure 2b and Supporting Information). Measurement of DNA double or single-strand breaks using an alkaline comet assay showed that cisplatin significantly increased comet tail moment ($P < 0.001$), while no significant difference was observed between A2780 cells treated with Ir catalyst **1** and untreated (negative control) cells (Figure 2c and Supporting Information). As such, while Ir-DNA interactions cannot be excluded with certainty, it is unlikely that DNA is a primary target of catalyst **1**.

Glutathione conjugation is a commonly identified deactivation pathway for therapeutic metallodrugs, including cisplatin. Surprisingly, the antiproliferative activity of catalyst **1** was not significantly affected by coadministration with L-buthionine sulfoximine, a selective inhibitor of glutamyl cysteine synthetase, which is known to deplete intracellular glutathione (IC_{50} = 20.9 ± 0.7 and 21.7 ± 0.9 μM, in the absence and presence of L-BSO, respectively). The apparent lack of deactivation by glutathione may be attributed to the slower ligand exchange kinetics of the low-spin d^6 Ir(III) metal ion compared to other transition metal catalysts, for example d^8 Pt(II), but further investigation in this regard is beyond the scope of this study.

When administered alone, catalyst **1** offers modest selectivity for cancer cells over noncancerous cell lines (MRC5 lung fibroblasts or MCF10-A non-tumorigenic breast cells). Selectivity for cancer cells over noncancerous cells (usually considered to be greater than one order of magnitude) is uncommon for Ir(III) catalysts, though some have been reported to exhibit up to 15 × selectivity towards cancer cells.[21] The modest selectivity of catalysts **1–3** is similar to other structurally similar Ir piano-stool catalysts bearing BINAP (2,2′-bis(diphenylphosphino)-1,1′-binaphthyl) and phenyl pyridine ligands.[4g,22] Nonetheless, in this study we hypothesize that catalytic modulation by coadministration of a hydride source may overcome this limitation.

Further accumulation studies were undertaken with catalyst **1** in A2780 ovarian cancer cells (Supporting Information). Temperature-dependent accumulation measurements (1 × IC_{50}, 3–6 h exposure) revealed lower Ir accumulation at 277 K compared to 310 K, suggesting the involvement of both energy-dependent and energy-independent mechanisms of Ir influx. Concentration-dependent accumulation studies (24 h, 310 K, no recovery time) revealed a linear relationship between dose and

Table 2. Antiproliferative activities of Ir TsDPEN catalysts **1**–**3** and cisplatin towards 13 human cell lines. Cells were exposed to test compounds for 24 h and allowed 72 h recovery time in drug-free medium. Cell viability was determined using the sulforhodamine B assay.[20] Data are reported as the average of two independent triplicate experiments (duplicate of triplicate) with the associated standard deviation of the average measurement. N.D. = not determined.

	Antiproliferative Activity (IC_{50})/μM			
Cell Line	**1** (Cp^*)	**2** (Cp^{xPh})	**3** (Cp^{xBip})	**Cisplatin**
A2780 (ovarian cancer)	20.9 ± 0.7	14 ± 2	10.2 ± 0.6	1.2 ± 0.3
A2780cis (ovarian, cisplatin-resistant)	17 ± 2	18 ± 1	6.3 ± 0.8	13.4 ± 0.3
A549 (lung cancer)	38 ± 2	25.2 ± 0.3	17 ± 3	3.2 ± 0.1
HCT116 (colorectal cancer)	40.3 ± 0.7	58.2 ± 0.9	15.0 ± 0.1	5.2 ± 0.3
HCT116-p21-/- (colorectal cancer, p21 knockout)	62.4 ± 0.3	N.D.	N.D.	9.2 ± 0.5
HCT116-p53-/- (colorectal cancer, p53 knockout)	63 ± 2	N.D.	N.D.	36.7 ± 0.3
MCF10-A (breast, non-tumorigenic)	42 ± 3	N.D.	N.D.	6 ± 1
HOF (ovarian, non-tumorigenic)	19.0 ± 0.1	26.8 ± 0.6	15.0 ± 0.7	10.2 ± 0.7
MCF7 (breast cancer)	14.6 ± 0.2	8 ± 1	3.7 ± 0.7	6.6 ± 0.4
MCF7-TAMR1 (breast, tamoxifen-resistant)	17.8 ± 0.6	N.D.	N.D.	6.0 ± 0.7
MRC5 (lung, non-tumorigenic)	17.3 ± 0.4	11.9 ± 0.9	5.9 ± 0.2	12.8 ± 0.5
OE19 (esophageal cancer)	>50	33.2 ± 0.5	12.9 ± 0.3	9 ± 1
PC3 (prostate cancer)	35.1 ± 0.6	18.8 ± 0.2	12 ± 1	4.1 ± 0.5

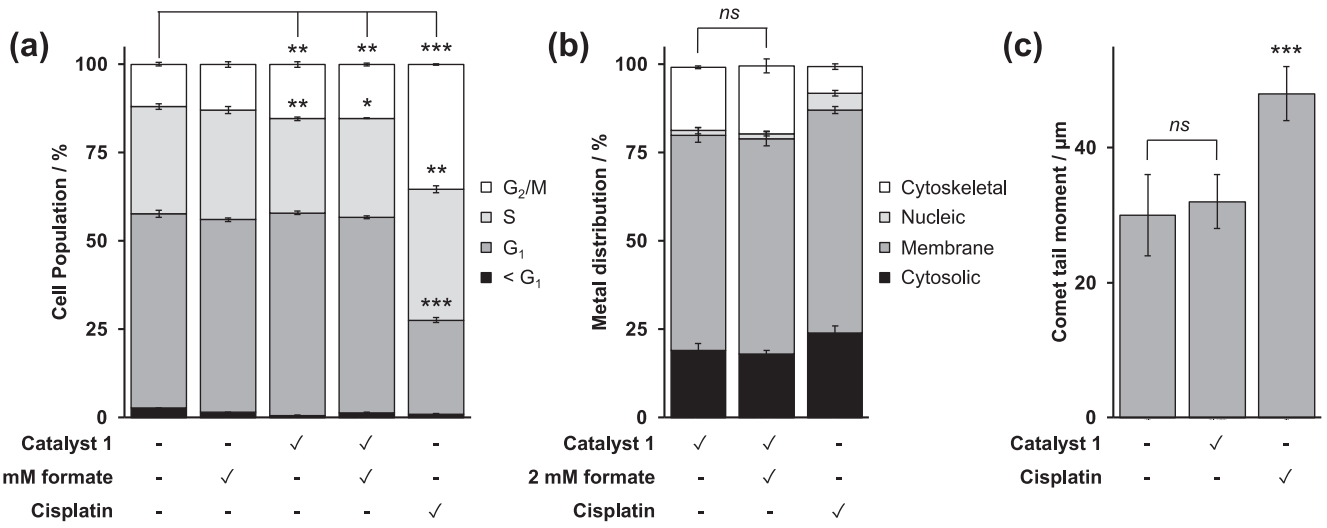

Figure 2. Mechanistic investigation of A2780 cancer cells treated with Ir catalyst **1**. (a) Cell cycle analysis: cells were either untreated or treated with Ir catalyst **1** (20 μM, 1 × IC_{50}) ± 2 mM sodium formate or an equipotent concentration of cisplatin (1 μM, 1 × IC_{50}) for 24 h without recovery time. Cells were fixed, stained using propidium iodide, and analyzed by flow cytometry in technical triplicate ($N = 3$). (b) Cellular metal distribution (fg Ir/cell) treated with Ir catalyst **1** ± 2 mM sodium formate, or cisplatin, at 1 × IC_{50} for 24 h. Cell pellets were fractionated using the FractionPREP fractionation kit (BioVision), resulting in four fractions: (i) cytosolic, (ii) membrane/organelle, (iii) nucleic, and (iv) cytoskeletal fractions. Metal content in each fraction was determined using ICP-MS after acidic digestion, and data were reported as % distribution (with associated standard deviation, $N = 3$) relative to the sum of the metal content across all four fractions. (c) Comet assay: cells were either untreated, treated with Ir catalyst **1** (20 μM, 1 × IC_{50}) or an equipotent concentration of cisplatin (1 μM, 1 × IC_{50}) for 24 h without recovery time. Cells were lysed under alkaline conditions and electrophoresis was carried out, DNA was stained using propidium iodide, and comet images ($N = 20$) were acquired by fluorescence microscopy. Statistical significances were tested using a two-tailed unpaired *t*-test assuming unequal sample variances (Welch's *t*-test). $^*P < 0.05$, $^{**}P < 0.01$, $^{***}P < 0.001$. NS = not statistically significant. Full numerical and statistical data are available in the Supporting Information.

intracellular Ir accumulation, while time-dependent measurements revealed that maximal Ir accumulation is achieved within 3 h of exposure and does not decrease within the 24 h exposure time. This supports the further development of catalyst **1** as an in-cell catalyst and contrasts with the accumulation of a structurally similar isoelectronic Os catalyst [Os(*p*-cymene)(TsDPEN)] which reached maximal intracellular Os accumulation after 6 h and then decreased irrespective of the extracellular Os concentration.[5a]

Catalyst **1** is known to catalyze transfer hydrogenation reactions in organic solvents, using formic acid as a sacrificial hydride donor (itself becoming irreversibly converted to carbon dioxide).[14] To catalyze transfer hydrogenation reactions in aqueous media, the sodium salt of formic acid was selected

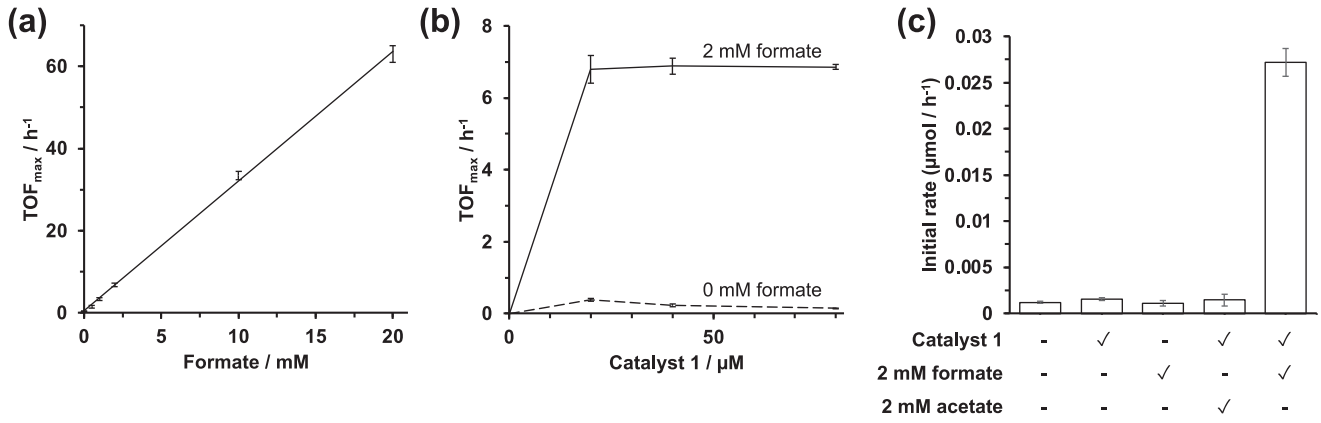

Figure 3. Catalytic reduction of 2,6-dichlorophenolindophenol (2,6-DCPIP, blue) to its colorless reduced form by Ir catalyst **1** and sodium formate (hydride donor, 0–20 mM) in phosphate buffered saline (containing 1% v/v dimethyl sulfoxide to aid catalyst solubility). 2,6-DCPIP concentration was determined by UV–vis spectroscopy (λ = 600 nm) using a 3-point calibration (Supporting, Figure S3). TOF_{max} = maximal turnover frequency. Data are reported as the average of three independent experiments (N = 3) with an associated standard deviation. Full numerical information can be found in the Supporting Information.

as a hydride donor since formate is a naturally occurring metabolite.[23] Determination of the acute toxicity (LC_{50}) in the zebrafish embryo model showed sodium formate to be nontoxic at millimolar concentrations (LC_{50} = 19.4 ± 0.6 mM). Formate is rapidly absorbed in humans and reaches peak plasma levels within 10–30 min post-administration, with negligible change in blood pH, followed by rapid elimination (plasma $t_{\frac{1}{2}}$ = 45 min).[24] Nonetheless, formate may be involved in the pathology of defective one-carbon metabolism,[23] so further clinical safety evaluation remains necessary.

Catalytic activity was assessed using the water-soluble redox probe 2,6-dichlorophenolindophenol (2,6-DCPIP) as a substrate for transfer hydrogenation (Figure 3). 2,6-DCPIP is commonly used to measure photosynthetic rates: oxidized 2,6-DCPIP is blue (λ_{max} = 600 nm), while its reduced amino-phenol form is colorless. The reduction of 2,6-DCPIP to its colorless form by catalyst **1** (20 µM, equivalent to 1 × IC_{50} in A2780 cells) and 2 mM sodium formate was successful in phosphate buffered saline solution containing 1% *v/v* dimethyl sulfoxide to aid catalyst solubility, achieving a maximum turnover frequency (TOF_{max}) of 6.8 ± 0.4 h^{-1}. To ensure 2,6-DCPIP was directly reduced by catalyst **1** and sodium formate (as opposed to indirectly reporting redox modulation of another reaction component), experiments were repeated substituting 2,6-DCPIP for two alternative colorimetric redox indicators: Alamar Blue (reduction of blue resazurin N-oxide to pink resorufin phenoxazine) or 3-(4,5-dimethylthiazol-2-yl)-2,5-diphenyltetrazolium bromide (MTT – reduction of yellow tetrazolium to purple formazan), neither of which displayed any change in absorbance in the presence of catalyst **1** and sodium formate. Increasing the concentration of sodium formate significantly improved the rate of 2,6-DCPIP reduction (20 µM catalyst and 20 mM sodium formate TOF_{max} = 63 ± 2 h^{-1}, Figure 3a) while increasing only the catalyst concentration had no effect on the rate of 2,6-DCPIP reduction (80 µM catalyst and 2 mM sodium formate TOF_{max} = 6.85 ± 0.07 h^{-1}, Figure 3b). Importantly, no reduction in 2,6-DCPIP absorbance (λ_{max} = 600 nm) was observed in the absence of catalyst, nor upon substitution of sodium formate for sodium acetate (which cannot donate hydride) confirming the specific role of both Ir catalyst **1** and sodium formate (Figure 3c).

With an aqueous-compatible transfer hydrogenation catalyst in hand, in-cell activity modulation experiments were carried out by coadministering Ir catalyst **1** with nontoxic concentrations of sodium formate (0–2 mM) to A2780 ovarian cancer cells (Figure 4 and Supporting Information). This combination of catalyst and hydride donor resulted in a 75% decrease in cell survival relative to the sodium formate-free control (P = 0.0040). Measurement of cofactor-dependent Ir accumulation in cells demonstrated that potency modulation was not caused by increased Ir uptake (no cofactor: 33.4 ± 0.5 fg·cell^{-1}, with 2 mM formate: 34.9 ± 0.6 fg cell^{-1}, P = 0.22). Similarly to 2,6-DCPIP experiments, the specific role of the formate anion for in-cell transfer hydrogenation was confirmed by substitution for sodium acetate, a chemically similar carboxylate that cannot act as a suitable hydride donor and did not significantly reduce A2780 cell survival compared to the acetate-free control (P = 0.4572). The catalytic modulation of cell survival by Ir catalyst **1** and sodium formate was conserved in MCF7 breast cancer cells (60% reduction in cell viability in the presence of 2 mM formate, P = 0.0027), as well as in two drug-resistant cell lines A2780cis (cisplatin-resistant) and MCF7-TAMR1 (tamoxifen-resistant), achieving 53% (P = 0.0082) and 75% (P = 0.0012) reductions in viability, respectively, relative to the sodium formate-free control (Supporting Information Table S9 and Figure S6). As such, in-cell catalysis appears to offer potential as a novel strategy to overcome drug resistance. Crucially, no catalytic modulation of cell survival was observed in noncancerous MRC5 cells (Figure 4, P = 0.3827 compared to sodium formate-free control). This suggests that such a catalytic mechanism of action in cells generates selectivity for cancer cells over non-cancerous cells, supporting previous findings using both Ru(II) and Os(II) in-cell catalysts.[1a,5a]

To develop a more comprehensive understanding of the mechanism of action of Ir catalyst **1**, iridium speciation in human serum was investigated using anion exchange (AEX) chromatography coupled to offline ICP-MS quantification and SDS-PAGE. Ir was observed in two distinct regions of the LC-ICP-MS chro-

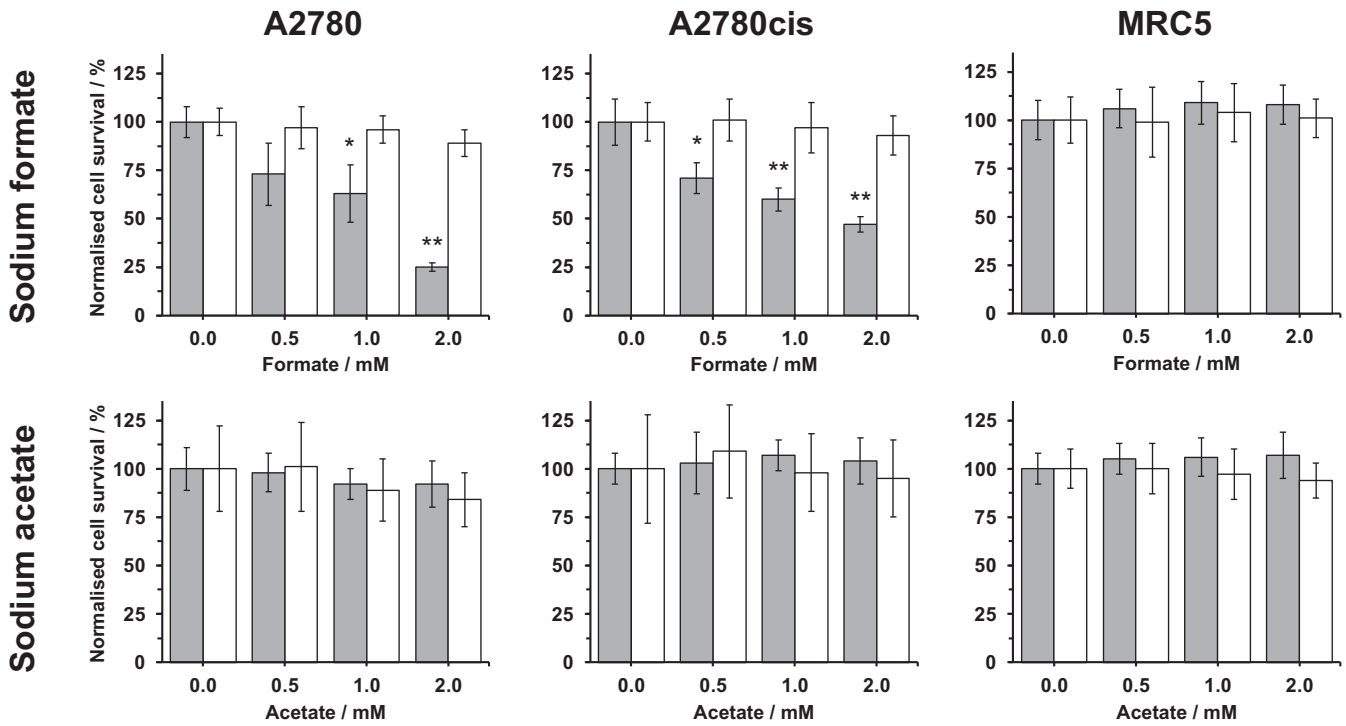

Figure 4. Activity modulation of Ir Cp* catalyst **1** in cells: A2780 ovarian cancer cells, A2780cis cisplatin-resistant ovarian cancer cells, and MRC5 noncancerous human lung fibroblasts. Cells were treated in the presence (grey bars) or absence (white bars) of catalyst **1** (1.0 × IC_{50}) with coadministration of a nontoxic concentration of either sodium formate (0–2 mM, upper) or sodium acetate (0–2 mM, lower). Experiments were carried out in triplicate as part of two independent experiments. Statistical significances (Welch's *t*-test) were determined relative to the co-factor free (0 mM) control. $^{*}P < 0.05$, $^{**}P < 0.01$, $^{***}P < 0.001$. Full numerical and statistical data can be found in the Supporting Information.

matogram: t_R = 1–2 min (4.8% of the total recovered Ir) and t_R = 10.5–12.5 min (75.7% of the total recovered Ir). SDS-PAGE revealed the latter to contain a highly abundant serum protein (R_f = 0.517, ~70 kDa), likely to be albumin (66.5 kDa, pI = 5),[25] which is well known to transport metal ions and has been shown to reversibly bind structurally similar half-sandwich Ir(III), Os(II), Ru(II), and Ru(III) catalysts.[26] Albumin has also attracted interest for development as a drug delivery vehicle,[27] and its conjugates with the Ru(III) metallodrug NAMI-A promote prolonged activity and selective accumulation in tumor cells.[26,28] The earlier iridium-containing fraction (t_R = 1–2 min) contained an abundant ~50 kDa protein (R_f = 0.570), which is likely attributable to the IgG heavy chain (50 kDa, pI = 6.4–7.6).[29] Though there are few examples of metallodrug-IgG interactions, a Ru(II) pyrithione catalyst has been reported to exhibit a similar protein binding distribution (IgG = 5% Ru, albumin = 70% Ru, unbound = 25% Ru).[30] Nevertheless, given Ir was quantified at a short retention time (t_R = 1–2 min), it remains unclear whether Ir was bound to either IgG or another protein of a similar size, nonprotein bound Ir (for example, elution of the neutral Ir(III) TsDPEN catalyst), or Ir bound to a protein of different size that was not resolved by Coomassie staining. Further investigations into Ir extracellular speciation, while stimulating, were however beyond the scope of this in-cell catalysis study.

Since the catalyst appeared to be redox-targeting, levels of intracellular ROS were quantified using confocal fluorescence microscopy using the membrane-permeable probe 2′,7′-dichlorodihydrofluoescein diacetate (H_2-DCFDA) (Figure 5a). This reagent is oxidized intracellularly to produce dichlorofluorescein (DCF), which exhibits a green fluorescence. A2780 cells were co-stained using 4′,6-diamidino-2-phenylindole (DAPI), which exhibits blue fluorescence when bound to double-stranded DNA, providing a marker for cell localization. Assay suitability was confirmed by the positive control (1 μM hydrogen peroxide, 1 h), which generated a significant increase in green fluorescence (23 ± 3 RFU, P = 0.0078) compared to the untreated control (2.7 ± 0.9 RFU). Treatment of cells with Ir catalyst **1** (1 × IC_{50}, 24 h) significantly increased green fluorescence (11 ± 3 RFU, P = 0.0443) relative to the untreated control; however, the combination of Ir catalyst **1** and sodium formate (3 ± 1 RFU) remained statistically similar to the untreated control (P = 0.7251). When administered to cells alone, Ir catalyst **1** generated oxidative stress, which was negated (due to the reduction catalysis mechanism) when co-administered with a suitable hydride source (Figure 5b).

To explore whether the generation of ROS by Ir catalyst **1** was conserved in vivo, zebrafish embryos were treated with **1** (1 × LC_{50}, 10 μM) for 96 h and stained using H_2-DCFDA.[10] The suitability of H_2-DCFDA as a probe for in vivo ROS detection was confirmed using pyocyanin, a known inducer of ROS in zebrafish,[31] as a positive control to validate experimental conditions. Basal ROS levels associated with normal physiological pathways were observed in the untreated (stained) control, while 510 nm fluorescence was significantly enhanced in embryos incubated in the presence of either pyocyanin or catalyst **1** (Figure 5c). The in vivo distribution of ROS in embryos treated

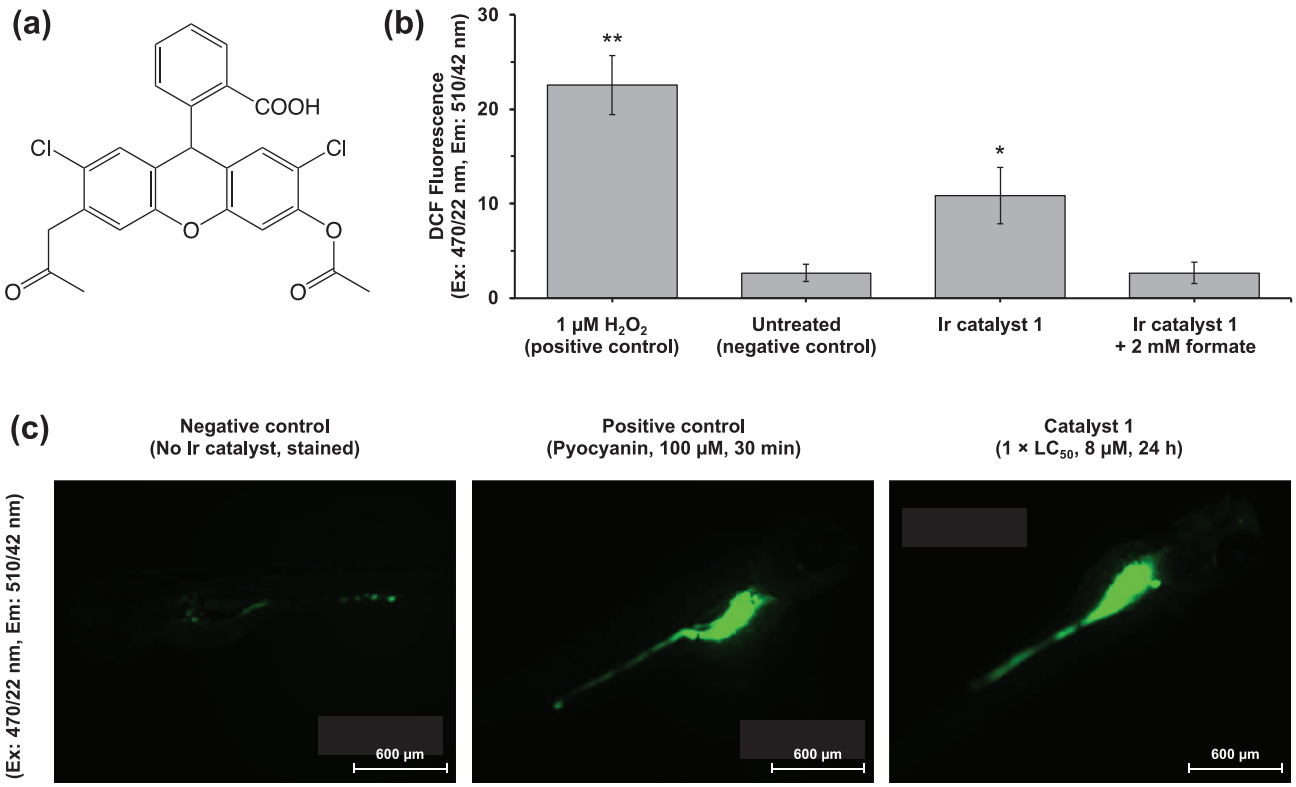

Figure 5. (a) Structure of green-fluorescent ROS probe 2′,7′-dichlorodihydrofluoescein diacetate (H_2-DCFDA). (b) DCF fluorescence in A2780 cancer cells which were either untreated (stained), or treated with 1 μM hydrogen peroxide (H_2O_2, positive control), Ir catalyst **1** (1 × IC_{50}) or Ir catalyst **1** (1 × IC_{50}) + 2 mM sodium formate for 24 h, performed as part of three technical biological replicates ($N = 3$). (c) Fluorescence microscopy detection of in vivo ROS production by catalyst **1** in zebrafish (*Danio rerio*) embryos using H_2-DCFDA. Zebrafish embryos were treated with catalyst **1** (1 × LC_{50}, 8 μM, 96 h), a positive control to confirm assay validity (pyocyanin, 100 μM, 30 min) or were untreated control, showing basal signaling levels of ROS. Statistical significances were testing using a two-tailed unpaired *t*-test assuming unequal sample variances (Welch's *t*-test). $^*P < 0.05$, $^{**}P < 0.01$, $^{***}P < 0.001$.

with Ir catalyst **1** was consistent with previous ROS distribution in zebrafish generated by a structurally similar Os(II) redox catalyst,[10] localized in the swim bladder of the embryo.

3. Conclusions

Ir(III) tosyl-diamine transfer hydrogenation catalysts with low in vivo toxicity have been studied for selective targeting of cancer cells and overcoming drug resistance. These catalysts exploit a unique redox-targeting mechanism of action that is distinct from traditional DNA-binding therapeutics and may offer a new approach to chemotherapeutic design. Catalytic performance under biologically relevant conditions revealed that the amount of the hydride source formate was rate-limiting, challenging the hypothesis that the main barrier to achieving in-cell transfer hydrogenation is the delivery and availability of the catalyst itself. Ir catalysts showed lower in vivo acute toxicity in zebrafish embryos than previously reported Os(II) analogues, and in-cell catalytic activity was maintained in both cisplatin (ovarian) and tamoxifen (breast) drug-resistant cells. In vitro generation of oxidative stress was shown to be formate-dependent, providing further evidence to support the proposed transfer hydrogenation mechanism in cells. Future work in this field will involve exploring delivery mechanisms and/or formulation strategies that enhance hydride source availability, as well as alternative biologically compatible hydride sources that could be administered at higher concentrations.

4. Materials and Methods

Synthetic methods to prepare iridium dimer precursors $[Ir(Cp^*)Cl_2]_2$, $[Ir(Cp^{xPh})Cl_2]_2$, and $[Ir(Cp^{xBip})Cl_2]_2$ have been previously reported,[32] and are also commercially available. Iridium Cp^{xPh} and Cp^{xBip} dimer precursors were kindly provided by Dr Abraha Habtemariam (University of Warwick). Organic and deuterated solvents, triethylamine, sodium and potassium hydroxides, propidium iodide, Tris (99.9999% trace metal basis), ammonium acetate (99.9999% trace metal basis), 2,6-dichlorophenolindophenol, cisplatin, trichloroacetic acid, sodium formate, and sodium acetate were purchased from Merck and used as received unless specified. (1*R*,2*R*)-1,2-bis(4-methoxyphenyl)ethylenediamine dihydrochloride was purchased from Alfa Aesar. (*R*,*R*)-TsDPEN and (*S*,*S*)-TsDPEN were purchased from Arran Chemicals (Ireland). Inorganic Ventures certified reference materials for ICP-MS analysis (^{193}Ir and ^{195}Pt, 1000 mg L^{-1}) were purchased from ESS Lab (Essex, UK). Dulbecco's Modified Eagle Medium (DMEM, high glucose without sodium pyruvate, D5796), trypsin/EDTA (0.25% in HBSS, T4049), Dulbecco's phosphate buffered saline (DPBS without Ca^{2+} or Mg^{2+}, D8537), penicillin-streptomycin (10,000 units penicillin and

10 mg mL^{-1} streptomycin in 0.9% NaCl, P0781) and fetal calf serum (non-USA origin, F9665) were purchased from Merck Life Sciences and used as received. 4–15% mini-protean TGX precast gels, Coomassie stain, tris/glycine/SDS running buffer, and Precision Plus unstained protein ladder were purchased from Bio-Rad Laboratories. Laemmli buffer was purchased from Scientific Laboratory Supplies (Nottingham, UK). Centrifuge tubes (Corning CentriSTAR 15 and 50 mL tubes) were purchased from Appleton Wood Limited (Birmingham, UK). Sterile pipette tips were purchased from Starlab (UK). C-Chip disposable hemocytometers were purchased from Cambridge Biosciences. All other cell culture plasticware (Greiner GmbH) was purchased from Scientific Laboratory Supplies (Nottingham, UK). All other non-specified reagents were purchased from Merck and used as received.

A2780, A2780cis, A549, HCT116, HCT116-p21-/-, HCT116-p53-/-, MCF7, MCF7-TAMR1, MRC5, OE19, and PC3 cells were obtained from the European Collection of Authenticated Cell Cultures (ECACC). MCF10-A cells were obtained from LGC Standards Limited (Teddington, UK). Human ovarian fibroblast (HOF) cells were obtained from Caltag Medsystems (Buckingham, UK).

4.1. Synthesis of Ligand L1 and Ir(III) Catalysts 1–6

Ligand L1: Methoxyphenyl diamine ligand **L1** was prepared from (1*R*,2*R*)-1,2-bis(4-methoxyphenyl)ethylenediamine dihydrochloride (380 mg, 1.10 mmol) dissolved in anhydrous dichloromethane (50 mL) cooled in an ice bath. Triethylamine (0.23 mL, 1.65 mmol) was added under an inert nitrogen atmosphere with stirring before slowly adding a solution of *p*-toluene sulfonyl chloride (210 mg, 1.10 mmol) in dry dichloromethane (80 mL) dropwise. The ice bath was removed, and the solution was allowed to warm to ambient temperature for 1 h. The organic phase was washed with water (3 × 15 mL), dried over magnesium sulfate, and the solvent removed in vacuo to afford a light-yellow oil. The product was recrystallized from hot diethyl ether and washed with additional ice-cold diethyl ether to afford an amorphous white solid (363 mg, 0.85 mmol, 74%). ^{1}H NMR (500 MHz, $CDCl_3$, TMS): $\delta = 7.32$ (2H, d, $^3J = 8.1$ Hz, ArH), 7.04 (2H, br. s, ArH), 6.98 (4H, d, $^3J = 7.7$ Hz, SO_2ArH), 6.67 (4H, d, $^3J = 8.1$ Hz, ArH), 4.34 (1H, br. s, TsNHCH), 4.10 (1H, d, $ArCHNH_2$), 3.73 (3H, br. s, OCH_3), 3.70 (3H, s, OCH_3), 2.32 (3H, s, SO_2ArCH_3), 1.81 (2H, br. s, NH_2); ^{13}C NMR (125 MHz, $CDCl_3$, TMS): $\delta = 158.8$, 142.4, 137.3, 129.0, 128.6, 127.0, 113.7, 113.6, 55.2, 55.1, 45.8, 21.4; UV–vis: λ_{max} 275 and 285 nm. HRMS (*m/z*): [M + Na]+ calculated for $C_{23}H_{26}N_2NaO_4S$: 449.1511; found 449.1503; analysis% (calculated for $C_{23}H_{26}N_2O_4S$, found): C (64.77, 64.46), H (6.14, 6.10), N (6.57, 6.60).

Catalyst 1 [Ir(Cp*)((R,R)-TsDPEN)]: Catalyst **1** has been previously reported using a different synthetic method.[14] In this work, catalyst **1** was prepared by combining $[Ir(Cp^*)Cl_2]_2$ (120 mg, 0.15 mmol) and (*R*,*R*)-(H)TsDPEN (110.6 mg, 0.30 mmol) in chloroform (10 mL) with freshly ground KOH (168 mg, 3 mmol). A color change from orange to purple was observed in <1 min. After 5 min, water (10 mL) was added with stirring for a further 10 min. The organic layer was removed and concentrated in vacuo to yield a purple oil, which was dissolved in the minimum amount of dichloromethane, followed by precipitation with *n*-pentane. The product was collected as a purple crystalline solid (144 mg, 0.21 mmol, 69%). ^{1}H NMR (400 MHz, $CDCl_3$, 25 °C, TMS): $\delta = 7.55$ (d, ^3J(H,H) = 7.4 Hz, 2H), 7.06–7.36 (m, 10H), 6.79 (d, ^3J(H,H) = 8.0 Hz, 2H), 5.34 (s, 1H; CHNTs), 4.15 (br. d, 1H; CHNH), 2.24 (s, 3H; CH_3), 1.92 (s, 15H; Cp*); ^{13}C NMR (100 MHz, $CDCl_3$, 25 °C, TMS): $\delta =$ 128.2, 127.8, 127.6, 126.9, 126.6, 126.5, 126.2, 85.2, 80.3, 74.1, 10.2; UV–vis: λ_{max} 429 and 536 nm; HRMS (*m/z*): $[M + H]^+$ calculated for $C_{31}H_{36}IrN_2O_2S$, 693.2121; found, 693.2118; analysis % (calculated for $C_{31}H_{35}IrN_2O_2S$, found): C (53.81, 53.80), H (5.10, 5.09), N (4.05, 4.02).

Catalyst 2 [Ir(Cp^{xPh})((R,R)-TsDPEN)]: This catalyst was obtained following the method described for catalyst **1** using dimer $[Ir(Cp^{xPh})Cl_2]_2$ (50.3 mg, 0.055 mmol) and (*R*,*R*)-(H)TsDPEN (40 mg, 0.11 mmol). The product was isolated as a dark purple amorphous solid (50 mg, 0.066 mmol, 61%). ^{1}H NMR (500 MHz, $CDCl_3$, 25 °C, TMS): $\delta = 7.58$ (d, ^3J(H,H) = 7.5 Hz, 2H), 7.08–7.53 (m, 15H), 6.79 (d, ^3J(H,H) = 8.0 Hz, 2H), 5.67 (br. d, ^3J(H,H) = 4.0 Hz, 1H; NH), 4.42 (s, 1H; CHNTs), 4.20 (d, ^3J(H,H) = 4.0 Hz, 1H; CHNH), 2.25 (s, 3H; CH3), 2.07 (s, 3H; Cp^{xPh}), 2.02 (s, 3H; Cp^{xPh}), 1.89 (s, 3H; Cp^{xPh}), 1.88 (s, 3H; Cp^{xPh}); ^{13}C NMR (125 MHz, $CDCl_3$, 25 °C, TMS) $\delta =$ 146.7, 146.5, 141.1, 140.1, 131.5, 130.9, 128.6, 128.2, 127.9, 127.7, 126.9, 126.7, 126.6, 126.3, 89.8, 88.0, 87.5, 84.8, 83.8, 80.5, 74.2, 21.2, 10.7, 10.6, 10.5, 10.3; UV–vis: λ_{max} 432 and 547 nm; HRMS (*m/z*): $[M + H]^+$ calculated for $C_{36}H_{38}IrN_2O_2S$, 755.2278; found, 755.2268; analysis % (calculated for $C_{36}H_{37}IrN_2O_2S$, found): C (57.35, 56.94), H (4.95, 4.96), N (3.72, 3.70).

Catalyst 3 [Ir(Cp^{xBip})((R,R)-(TsDPEN)]: This catalyst was obtained following the method described for catalyst **1** using dimer $[Ir(Cp^{xBip})Cl_2]_2$ (58.6 mg, 0.055 mmol) and (*R*,*R*)-(H)TsDPEN (40 mg, 0.11 mmol). The product was isolated as a dark purple crystalline solid (33 mg, 0.040 mmol, 37%). ^{1}H NMR (500 MHz, $CDCl_3$, 25 °C, TMS): $\delta =$ 7.52–7.64 (m, 8H), 7.44–7.50 (m, 2H), 7.35–7.42 (m, 1H), 7.07–7.30 (m, 10H), 6.80 (d, ^3J(H,H) = 8.0 Hz, 2H; ArH), 5.67 (d, ^3J(H,H) = 4.0 Hz, 1H; NH), 4.43 (s, 1H; CHTs), 4.22 (d, ^3J(H,H) = 4.0 Hz, 1H; CHNH), 2.25 (s, 3H; CH3), 2.09 (s, 3H; Cp^{xBip}), 2.03 (s, 3H; Cp^{xBip}), 1.94 (s, 3H; Cp^{xBip}), 1.93 (s, 3H; Cp^{xBip}); ^{13}C NMR (125 MHz, CDCl3, 25 °C, TMS) $\delta =$ 146.7, 146.5, 141.1, 141.0, 140.4, 140.1, 131.3, 128.9, 128.6, 127.9, 127.7, 127.6, 127.3, 127.1, 127.1, 127.0, 126.7, 126.6, 126.3, 89.4, 88.1, 87.6, 84.8, 83.9, 80.6, 74.2, 21.25, 10.8, 10.6, 10.5, 10.3; UV–vis: λ_{max} 430 and 547 nm; HRMS (*m/z*): $[M + H]^+$ calculated for $C_{42}H_{42}IrN_2O_2S$, 831.2592; found, 831.2599; analysis % (calculated for $C_{42}H_{41}IrN_2O_2S$, found): C (60.77, 61.21), H (4.98, 5.07), N (3.37, 3.34).

Catalyst 4 [Ir(Cp*)((R,R)-TsDPEN)]: This catalyst was obtained following the method described for catalyst **1** using dimer $[Ir(Cp^*)Cl_2]_2$ (46.7 mg, 0.06 mmol) and diamine ligand **L1** (50 mg, 0.12 mmol). The product was isolated as a dark purple amorphous solid (37.5 mg, 0.05 mmol, 41%). ^{1}H NMR (500 MHz, $CDCl_3$, 25 °C, TMS): $\delta = 7.44$ (d, ^3J(H,H) = 8.4 Hz, 2H; ArH), 7.25 (d, ^3J(H,H) = 8.2 Hz, 2H; ArH), 7.04 (d, ^3J(H,H) = 8.5 Hz, 2H; ArH), 6.82 (d, ^3J(H,H) = 8.0 Hz, 2H; ArH), 6.79 (d, ^3J(H,H) = 8.5 Hz, 2H; ArH), 6.65 (d, ^3J(H,H) = 8.6 Hz, 2H; ArH), 5.36 (br. s, 1H; NH), 4.18 (s, 1H;

TsNCH), 4.05 (s, 1H; CHNH), 3.78 (s, 3H; OCH_3), 3.78 (s, 3H; OCH_3), 2.26 (s, 3H; CH_3), 1.91 (s, 15H; CH_3); ^{13}C NMR (125 MHz, $CDCl_3$, 25 °C, TMS) δ = 158.5, 158.1, 140.9, 138.9, 138.7, 128.2, 127.1, 126.7, 113.1, 85.1, 79.8, 73.4, 55.3, 21.2, 10.2; UV–vis: λ_{max} 285, 430, and 538 nm; HRMS (*m/z*): $[M + H]^+$ calculated for $C_{33}H_{40}IrN_2O_4S$, 753.2333; found, 753.2336; analysis % (calculated for $C_{33}H_{39}IrN_2O_4S$, found): C (52.71, 53.03), H (5.23, 5.43), N (3.73, 3.65).

Catalyst 5 [Ir(Cp^{xPh})((R,R)-TsDPEN)]: This catalyst was obtained following the method described for catalyst **1** using dimer $[Ir(Cp^{xPh})Cl_2]_2$ (53.9 mg, 0.06 mmol) and diamine ligand **L1** (50 mg, 0.12 mmol). The product was isolated as a dark purple amorphous solid (35.5 mg, 0.04 mmol, 37%). ^1H NMR (500 MHz, $CDCl_3$, 25 °C, TMS): δ = 7.51 (d, ^3J(H,H) = 6.9 Hz, 2H; ArH), 7.47 (d, ^3J(H,H) = 8.5 Hz, 2H; ArH), 7.39 (br. s, 1H; NH), 7.32–7.38 (m, 3H; ArH), 7.28 (d, ^3J(H,H) = 8.2 Hz, 2H; ArH), 7.05 (d, ^3J(H,H) = 8.5 Hz, 2H; ArH), 6.82 (d, ^3J(H,H) = 7.9 Hz, 2H; ArH), 6.77 (d, ^3J(H,H) = 8.5 Hz, 2H; ArH), 6.65 (d, ^3J(H,H) = 8.5 Hz, 2H; ArH), 4.30 (s, 1H; CHNTs), 4.10 (s, 1H; CHNH), 3.79 (s, 3H; OCH_3), 3.78 (s, 3H; OCH_3), 2.26 (s, 3H; CH_3), 2.07 (s, 3H; CH_3), 2.02 (s, 3H; CH_3), 1.89 (s, 3H; CH_3), 1.88 (s, 3H; CH_3); ^{13}C NMR (125 MHz, $CDCl_3$, 25 °C, TMS) δ 158.6, 158.2, 141.2, 140.0, 138.8, 131.5, 130.9, 128.6, 128.2, 127.9, 127.2, 126.7, 113.1, 89.8, 87.9, 87.5, 84.6, 84.0, 80.0, 73.5, 55.3, 21.2, 10.7, 10.6, 10.5, 10.4; UV–vis: λ_{max} 278, 433, and 549 nm; HRMS (*m/z*): $[M + H]^+$ calculated for $C_{38}H_{42}IrN_2O_4S$, 815.2490; found, 815.2485; analysis % (calculated for $C_{38}H_{41}IrN_2O_4S$, found): C (56.07, 55.98), H (5.08, 5.31), N (3.44, 3.31).

Catalyst 6 [Ir(Cp^{xBip})((R,R)-TsDPEN)]: This catalyst was obtained following the method described for catalyst **1** using dimer $[Ir(Cp^{xBip})Cl_2]_2$ (62.2 mg, 0.06 mmol) and diamine ligand **L1** (50 mg, 0.12 mmol). The product was isolated as a dark purple amorphous solid (30.7 mg, 0.03 mmol, 28%). ^1H NMR (500 MHz, $CDCl_3$, 25 °C, TMS): δ = 7.61 (d, ^3J(H,H) = 7.5 Hz, 2H; ArH), 7.57 (d, ^3J(H,H) = 5.1 Hz, 2H; ArH), 7.44–7.51 (m, 4H; ArH), 7.39 (m, 2H; ArH), 7.30 (d, ^3J(H,H) = 8.0 Hz, 2H; ArH), 7.16 (d, ^3J(H,H) = 8.5 Hz, 1H; ArH), 7.07 (d, ^3J(H,H) = 8.4 Hz, 2H; ArH), 6.96–7.04 (br. s, 1H; NH), 6.84 (d, ^3J(H,H) = 8.0 Hz, 2H; ArH), 6.79 (d, ^3J(H,H) = 8.5 Hz, 2H; ArH), 6.66 (d, ^3J(H,H) = 8.5 Hz, 2H; ArH), 4.31 (s, 1H; CHNTs), 4.11 (s, 1H; CHNH), 3.79 (s, 3H; OCH_3), 3.78 (s, 3H; OCH_3), 2.27 (s, 3H; CH_3), 2.09 (s, 3H; CH_3), 2.04 (s, 3H; CH_3), 1.94 (s, 3H; CH_3), 1.93 (s, 3H; CH_3); ^{13}C NMR (125 MHz, $CDCl_3$, 25 °C, TMS) δ = 158.6, 158.2, 141.2, 141.0 140.4, 140.1, 138.8, 131.3, 128.9, 128.2, 127.9, 127.7, 127.3, 1271, 126.7, 113.6, 113.2, 113.1, 89.2, 88.0, 87.6, 84.7, 84.0, 80.0, 73.5, 61.2, 55.3, 21.2, 10.9, 10.7, 10.5, 10.4; UV–vis: λ_{max} 263, 431, and 548 nm; HRMS (*m/z*): $[M + H]^+$ calculated for $C_{44}H_{46}IrN_2O_4S$, 891.2803; found, 891.2800.

4.2. Physicochemical Experimentation

Stability in DMSO: Proton ^1H NMR spectra were obtained using a Bruker AV400 NMR spectrometer using DMSO-d_6 as solvent. Spectra were acquired after preparation (t = 21 min, allowing for sample preparation and instrument lock, shim, temperature, average point of acquisition) and after 24 h incubation at 37 °C. Data were analyzed using TopSpin version 4.4.0.

Aqueous stability: Stock solutions of catalyst **1**–**6** (3 mM) were prepared in phosphate buffered saline (300 μM final working concentration, 10% v/v DMSO to aid solubility). Samples were analyzed using a Shimadzu UV-2600 UV–vis Spectrophotometer (800–250 nm, slow scan speed, 1.0 nm sampling interval) immediately after preparation (t = 0 h) and after incubation at 37 °C (t = 24 h). Data were analyzed in Microsoft Excel.

Octanol–water partition coefficient (Log P) determination: Partition coefficients were determined by shake-flask method. Solutions of *n*-octanol-saturated water and water-saturated *n*-octanol were prepared by stirring equal volumes of each solvent for 24 h. To the water-saturated *n*-octanol was added enough catalyst to achieve a saturated solution, which was filtered using a 0.2 μm filter to remove undissolved particulates. This solution was combined with an equal volume of *n*-octanol-saturated water and shaken using an IKA Vibrax VXC basic shaker (1000 g min^{-1}, 24 h, room temperature). Next, solutions were allowed to separate for 1 h. Metal content (^{193}Ir) was determined in the aqueous layer before and after shaking using an Agilent 7900 series ICP-MS using an internal ^{166}Er standard in no-gas mode. Partition coefficients (Log P) were calculated as part of two independent experiments, each carried out in triplicate. Data were reported as the average of the two experiments with the associated standard deviation of the measurement.

Aqueous (cell free) catalysis using 2,6-dichlorophenolindophenol (DCPIP): Stock solutions of (i) catalyst **1**, sodium formate (hydride source) and 2,6-DCPIP were prepared in phosphate buffered saline (PBS) solution containing 1% v/v dimethyl sulfoxide to aid solubility. Solutions were combined to achieve final working concentrations of catalyst: 0–20 μM (equivalent to 1 × IC_{50} concentration in A2780 cells), sodium formate: 0–20 mM, and 2,6-DCPIP: 0–80 mM. Solutions were added independently to a 96-well plate, but within 1 min of each other. The substrate (2,6-DCPIP) was added at t = 0 h and defined the initiation of the reaction. This experiment included all appropriate control samples (catalyst alone, hydride source alone, 2,6-DCPIP alone, 2,6-DCPIP plus sodium formate). All experiments were carried out in triplicate (N = 3). Microplate absorbance was measured using an Omega FLUOstar microplate reader (600 nm) at ambient temperature (20 °C). UV–vis absorbance data were converted to molar concentrations using a 3-point calibration plot (Supporting Information. Figure S3). Initial reaction rates were determined within the first minute of data acquisition using Microsoft Excel and converted to TOF_{max} where the catalyst concentration was known. This experiment was repeated with the following modifications: (1) *specificity of the hydride source*: sodium formate (2 mM) was replaced by sodium acetate (2 mM). (2) *specificity of the substrate*: 2,6-DCPIP was replaced by Alamar Blue (reduction of blue resazurin *N*-oxide to pink resorufin phenoxazine) or 3-(4,5-dimethylthiazol-2-yl)-2,5-diphenyltetrazolium bromide (reduction of yellow tetrazolium to purple formazan).

Iridium extracellular speciation: A 1 mM solution of catalyst **1** was prepared in DMSO, which was diluted 100-fold with human

serum and incubated at 37 °C for 24 h prior to speciation analysis. After incubation, the sample was further diluted 10-fold using 50 mM Tris (Buffer A) for HPLC speciation analysis. Speciation was achieved using an Agilent Technologies Infinity II series HPLC fitted with a TSK gel Q-STAT anion exchange chromatography column (4.6 mm I.D. x 10 cm, 7 µM) and a UV–vis DAD detector (280 nm, referenced to 360 nm). After column equilibration with Buffer A, analysis was carried out with the following method parameters: 100 µL injection volume, linear gradient, 0.7 mL min^{-1} flow rate, 30 min run time, 10 MPa maximum pressure, pH 7.4, 25 °C. Elution gradient: 0.0–3.0 min, 0% Buffer B; 3.0–9.0 min, 20% Buffer B; 9.0–13.5 min, 50% Buffer B; 13.5–16.5 min, 100% Buffer B; 16.5–22.5 min, 100% Buffer B; 22.5–27.0 min, 0% Buffer B (re-equilibration); 27.0–30.0 min, 0% Buffer B. Eluent fractions (0.35 mL) were collected at 30 s intervals into centrifuge tubes for the first 20 min of analysis. The procedure was repeated five times and samples were pooled to obtain final fraction volumes of 1.75 mL. HPLC data were acquired and processed using Agilent CDS software version 2.7. Fractions were subject to two separate analysis methods: (1) ICP-MS quantification of ^{193}Ir was achieved using freshly prepared calibration standards in 50 mM Tris base (Buffer A) ranging from 0.1 to 1000 ppb. Data were acquired as instrumental triplicates using an Agilent 7900 Series ICP-MS with MassHunter 4.4 (Agilent Technologies) and processed using Microsoft Excel. (2) Protein identification was achieved using SDS-PAGE. Fifty microliters of each fraction were diluted two-fold with Laemelli buffer (50 µL) and vortexed to achieve a homogenous mixture before heating to 70 °C for 10 min. A Mini-Protean TGX Precast Gel was loaded with fractions 1–28 (retention time (t_R) = 0–14 min, 10 µL of denatured sample) alongside 10 µL of Precision Plus protein standard unstained ladder (0–250 kDa). Upon completion of electrophoresis, gels were removed and washed three times with Type I water, before staining using 50 mL Bio-Safe Coomassie G-250 stain for 48 h. Stained gels were subsequently rinsed for 30 min in Type I water. R_f values were calculated, and a calibration plot was constructed from ladder proteins (R_f as a function of molecular weight) to estimate the molecular weight of serum proteins (Supporting Information, Figure S4).

4.3. Biological Experimentation

Cell maintenance: All cell lines were grown as adherent monolayers in 75 cm^2 tissue culture flasks in a 5% CO_2 humidified atmosphere at 37 °C and passaged upon reaching 80%–90% confluence. All cell lines (except MCF10-A and HOF) were maintained in DMEM culture medium supplemented with 10% v/v fetal calf serum and 1% v/v penicillin/streptomycin antibiotics at 10,000 units. MCF10-A cells were maintained in DMEM/F12 medium supplemented with 5% v/v horse serum, human epidermal growth factor (20 ng mL^{-1}), hydrocortisone (0.5 mg mL^{-1}), cholera toxin (100 ng mL^{-1}), insulin (10 µg mL^{-1}), and 1% v/v penicillin/streptomycin antibiotics at 10,000 units. HOF cells were maintained in fibroblast medium supplemented (Cat. No. 2301, ScienCell) with 2% v/v fetal calf serum, 1% v/v penicillin/streptomycin and 1% fibroblast growth supplement (Cat. No. 2352, ScienCell). Drug-resistant cell lines (A2780cis and MCF7-TAMR1) were inoculated with drug (cisplatin or tamoxifen, respectively; 5 × IC_{50}, 24 h) every 10 passages to maintain resistance, and resistance was confirmed by antiproliferative activity screening in comparison to the sensitive parental cell line.

Antiproliferative activity screening: Briefly, 5 × 10^3 cells (A2780, A2780cis, A549, HCT116, HCT116-p21-/-, HCT116-p53-/-, HOF, MCF7, MCF7-TAMR1, MCF10-A, MRC5, OE19, or PC3) were seeded in flat-bottom 96-well plate and incubated for 48 h. A stock solution of test compound was prepared in DMEM, using 5% v/v DMSO to aid solubilization of the metallodrug. Serial dilutions of the test compound were performed to obtain six final working concentrations (typically 100, 50, 25, 10, 1, 0.1 µM, DMSO not exceeding 5% v/v). The supernatant medium was removed from wells by aspiration, and cells were treated (200 µL solution per well) for 24 h. After this time, the drug-containing supernatant was removed by aspiration, cells were washed with PBS (100 µL) and were allowed 72 h recovery time in drug-free medium (200 µL per well). Cell viability was determined using the sulforhodamine B colorimetric assay.[20] Cells were fixed by addition of 50% w/v trichloroacetic acid (50 µL per well) and incubated at 4 °C for 1 h. The supernatant was removed, and cells washed with water, before staining with sulforhodamine B solution (0.4% w/v sulforhodamine B solution prepared in 1% v/v acetic acid; 50 µL per well) for 1 h. Excess dye was removed by sequential washing with 1% v/v acetic acid, and then dye was re-solubilized by addition of 100 mM Tris base (200 µL per well). Absorbance was measured using an Omega FLUOstar microplate reader (492 nm). Data were normalized to untreated control wells, and sigmoidal dose/response curves were fitted using GraphPad Prism 10. Exact working concentrations of metal catalyst were accurately determined by ICP-OES analysis post biological experimentation. All experiments were carried out in duplicate of triplicate and final values reported are the average of each independent duplicate experiment with associated standard deviation. Statistical significances were evaluated using a two-tailed *t*-test assuming unequal samples variances (Welch's *t*-test) at the 95% confidence level.

Activity modulation in cells using sodium formate: Briefly, 5 × 10^3 cells (A2780, A2780cis, MCF7, MCF7-TAMR1, or MRC5) were seeded in flat-bottom 96-well plate and incubated for 48 h. After this time, cells were treated with catalyst and sodium formate to give final concentrations equal to 1.0 × IC_{50} (catalyst **1**) and 0–2 mM (sodium formate) respectively, which were added independently but within 5 min of each other, for 24 h. This included Ir-free controls for each concentration of sodium formate (0.0, 0.5, 1.0, or 2.0 mM) and a positive control of cisplatin (0–100 µM). After this time, cells were washed with PBS (100 µL) and were allowed 72 h recovery time in drug-free medium (200 µL per well). Cell viability was determined using the sulforhodamine B colorimetric assay as described for *Antiproliferative Activity Screening*.[20] Data were normalized relative to the sodium formate-free Ir control to demonstrate activity modulation by sodium formate. All experiments were carried out in duplicate

of triplicate and final values reported are the average of each independent duplicate experiment with associated standard deviation. Statistical significances were evaluated relative to the sodium formate-free Ir control, using a two-tailed *t*-test assuming unequal samples variances (Welch's *t*-test) at the 95% confidence level. This experiment was repeated with the following modification: sodium formate (0–2 mM) was exchanged for sodium acetate (0–2 mM).

Cellular iridium accumulation: Briefly, 4×10^6 cells (A2780, A2780cis, A549, HCT116, MCF7, MCF7-TAMR1, OE19, PC3) were seeded in P100 dishes and incubated for 24 h. After this time, cells were exposed to $1 \times IC_{50}$ equipotent concentrations of catalyst **1** (10 mL) for 24 h with no recovery time. The supernatant was removed by aspiration, cells were washed with PBS (10 mL) and harvested using trypsin/EDTA. A cell count was performed, and a cell pellet obtained by centrifugation (1000 rpm, 5 min, room temperature). The cell pellet was resuspended in PBS, transferred to an Eppendorf vial, and re-centrifuged under the same conditions. The supernatant was removed by aspiration and the cell pellet was digested by addition of 200 µL 72% v/v ultrapure nitric acid, which was incubated overnight at 80 °C. Ultrapure milli-Q water (Type I) was added to obtain a final working acid concentration of 3.6% v/v. Samples were analyzed using an Agilent 7900 series ICP-MS operated in no-gas and He-gas modes, using an internal standard of Er (50 ppb) and freshly-prepared matrix matched calibration standards for ^{193}Ir or ^{195}Pt (0–1000 ppb). Untreated (negative control) samples were obtained and measured for Ir content in triplicate to ensure methodological reliability. All experiments were performed in biological triplicate ($N = 3$) with further instrumental triplicate measurement of each biological replicate. Data were normalized by cell count and reported as an average femtograms Ir (fg Ir cell^{-1}) or Pt (fg Pt cell^{-1}) per cell with associated standard deviation. Statistical significances were evaluated using a two-tailed *t*-test assuming unequal samples variances (Welch's *t*-test) at the 95% confidence level. This experiment was also carried out with the following modifications: (1) *time-dependent accumulation*: cells were incubated in the presence of catalyst **1** ($1 \times IC_{50}$, 37 °C) for 3, 6, 18, or 24 h, or alternatively were incubated 24 h drug exposure followed by 24 h recovery in drug-free medium; (2) *temperature-dependent accumulation*: cells were incubated in the presence of catalyst **1** ($1 \times IC_{50}$) at 4 °C for 3 or 6 h. These experiments were carried out in parallel to 3–6 h incubation experiments at 37 °C to facilitate direct comparison; (3) *concentration-dependent accumulation*: cells were incubated 24 h at 37 °C using 0.25, 0.5, 1, or $1.5 \times IC_{50}$ concentrations of catalyst **1**; (4) *cofactor-dependent accumulation*: cells were treated with catalyst **1** (final concentration: $0.5 \times IC_{50}$) in the presence or absence of 2 mM sodium formate.

Cellular iridium distribution: Cell pellets were obtained as described for cellular iridium accumulation ($1 \times IC_{50}$ concentration ±2 mM sodium formate, 24 h, no recovery time) using either catalyst **1** or cisplatin. Cells were fractioned using the FractionPREP kit (BioVision) to obtain four fractions per sample: cytosol, membrane/organelle, nucleus, cytoskeleton; according to the manufacturer's instructions. Each fraction was independently analyzed for Ir using ICP-MS as described above (digestion with 72% v/v nitric acid, followed by dilution to obtain final working acid concentrations of 3.6% v/v). All experiments were performed in biological triplicate ($N = 3$) with further instrumental triplicate measurement of each biological replicate. Data were normalized to the sum of all four compartments and reported as average percentage distribution per fraction of the triplicate samples ($N = 3$) with associated standard deviation. Statistical significances were evaluated using a two-tailed *t*-test assuming unequal samples variances (Welch's *t*-test) at the 95% confidence level.

A2780 cell cycle analysis by flow cytometry: Cell pellets were obtained as described for cellular iridium accumulation ($1 \times IC_{50}$ concentration ±2 mM sodium formate, 24 h, no recovery time) using either catalyst **1** or cisplatin. Cell pellets were resuspended in 1 mL 80% v/v ethanol on ice for 1 h, before centrifugation (1000 rpm, 5 min). The supernatant was discarded, and cells were resuspended in a staining buffer containing propidium iodide (0.1% v/v from a 1 mg mL^{-1} DMSO stock) and 0.15% w/v ribonuclease A for 30 min on ice. The supernatant was removed by centrifugation (1000 rpm, 5 min) then the resulting cell suspension was filtered using a 70 µm cell strainer. Data were acquired using a Beckman Coulter CytoFLEX S flow cytometer using CytExpert software at the Technology Hub Flow Cytometry core facility (University of Birmingham) with analysis for propidium iodide using a yellow (561 nm) laser and PC5.5 filter (690/50 nm). Data were analyzed in FlowJo version 10.8.1 using the Watson (pragmatic) cell cycle fitting model and were reported as the average of three technical replicates ($N = 3$) with associated standard deviations. Statistical significance tested using an unpaired *t*-test assuming unequal variances (Welch's *t*-test) at the 95% confidence level.

A2780 reactive oxygen species (ROS) analysis by fluorescence microscopy: Cell pellets were obtained as described for cellular iridium accumulation ($1 \times IC_{50}$ concentration ± 2 mM sodium formate, 24 h, no recovery time). Positive control samples were treated with 1 mM hydrogen peroxide for 1 h prior to analysis to confirm assay suitability and performance. Samples were stained using 2′,7′-dichlorodihydrofluorescein diacetate (H_2-DCFDA, 0.1% v/v from a 1 mg mL^{-1} DMSO stock) and 4′,6-diamidino-2-phenylindole dihydrochloride (DAPI) solution in serum-free colorless cell culture medium for 45 min. After this time, cells were washed three times with PBS and data were acquired using an EVOS XL Core Imaging System at 10× magnification fitted with DAPI ($\lambda_{Ex} = 357/44$ nm, $\lambda_{Em} = 447/60$ nm) and GFP ($\lambda_{Ex} = 470/22$ nm, $\lambda_{Em} = 510/42$ nm) light cubes. Cells were located using DAPI and light transmission images, then mean green fluorescence intensity within the defined cell area was quantified using ImageJ version 1.54 for MacOS. This analysis was repeated for three independent biological replicates ($N = 3$). Statistical significances were evaluated using a two-tailed *t*-test assuming unequal samples variances (Welch's *t*-test) at the 95% confidence level.

Comet assay: This experiment was adapted from a procedure described by Olive et al.[33] Briefly, 1×10^6 A2780 cells were seeded in a 6-well plate and incubated for 24 h, after which time cells were treated with equipotent concentrations of Ir catalyst **1** or cisplatin, equal to $1 \times IC_{50}$, for 24 h without recovery time. Cells were harvested using trypsin/EDTA and a single cell suspension was obtained at a density of 2×10^4 cells mL^{-1}, which was mixed with low gelling temperature agarose (1% prepared in Type I water, 40 °C) and transferred to pre-prepared microscope slides (glass slides coated and dried with 1% low-gelling temperature agarose) at a density of 5×10^3 cells mL^{-1}. Slides were carefully submerged in basic lysis solution (0.1% sodium sarcosinate, 0.26 M NaOH, 1.2 M NaCl, and 100 mM Na_2EDTA in Type I water, 4 °C) for 24 h in the dark, and then washed in rinse solution (0.03 M NaOH and 2 mM Na2EDTA in Type I water) for 20 min. Electrophoresis was carried out in a horizontal chamber containing rinse solution at 20 V for 25 min, after which slides were washed with Type I water, stained with propidium iodide (2.5 $\mu g \cdot mL^{-1}$, 20 min, room temperature) and excess stain was removed by sequential water washing (3×10 mL). Comets were visualized ($N = 20$ per sample) using an EVOS XL Core Imaging System at 20× magnification fitted with a Texas Red ($\lambda_{Ex} = 585/29$ nm, $\lambda_{Em} = 628/32$ nm) light cube. At least 20 comets (comet head diameter, tail length, comet tail moment) were measured for each sample. Comets with a head diameter <20 μm were excluded. Data were analyzed using Microsoft Excel and reported as the average tail moment with associated standard deviation. Statistical significances were evaluated using a two-tailed *t*-test assuming unequal samples variances (Welch's *t*-test) at the 95% confidence level.

Acute in vivo toxicity in zebrafish (*Danio rerio*) embryos: Acute toxicities were determined as previously described.[10] Experiments were performed using Singapore wild-type zebrafish embryos (*D. rerio*) under 5 days postfertilization, under project license AWERB.10/16–17 and AWERB.85/21–22. All animals were maintained in accordance with ASPA 1986. The University of Warwick is a member of the Institute of Animal Technology and the Laboratory Animal Science Association, and all animal work carried out was approved by the University Ethical Review Committee. Singapore wild-type zebrafish were housed in 3.5 L tanks, monitored daily, and provided with food (live and powder) four times daily. Regular system checks were carried out daily to ensure water quality and parameters are maintained. Light cycle: 14 h day, 10 h night. Fish were mated once a week using two pairs per 1 L breeding tank. Embryos were collected and placed into petri dishes with fresh egg water. A stock solution of the catalyst was prepared in egg water, using DMSO to aid catalyst solubilization (final DMSO concentrations did not exceed 1% v/v in working solutions). Embryos were exposed to test solutions in 20 wells of a 24-well plate (one 24-well plate per concentration), which were seeded using at least one (and a maximum of three) embryos per well ($N = 20$). The remaining wells were treated with egg water only (untreated control). Plates were incubated for 96 h at 28.5 °C. At the end of the assay, embryo mortality was assessed by microscopy in accordance with OECD fish embryo acute toxicity text (OECD-236). Embryos exhibiting any one of the following traits were considered nonviable: (a) embryo coagulation, (b) absence of somite formation, (c) tail detachment, and (d) absence of a heartbeat. Dose-response curves were obtained by plotting % viable embryos against the logarithm of the drug concentration. Sigmoidal curves were fitted using GraphPad Prism 10. LC_{50} values were reported as the average ± standard deviation of two independent experiments ($N = 2$) each containing 20 replicates per concentration. Statistical significances were evaluated using a two-tailed *t*-test assuming unequal samples variances (Welch's *t*-test) at the 95% confidence level.

Localization of reactive oxygen species in zebrafish (*D. rerio*) embryos: Treated zebrafish embryos were obtained as part of LC_{50} screening assays (above). After 96 h exposure to catalyst **1** ($1 \times LC_{50}$, 8 μM), embryos were collected and washed with egg water to remove excess Ir catalyst. Separately, positive control embryos were treated with pyocyanin (100 μM, 30 min) a known in vivo ROS inducer to confirm assay performance or remained untreated (negative control). All embryos were anaesthetized using tricaine (0.2mg mL^{-1} in egg water, 30 min) after which time excess tricaine was removed by washing and embryos were stained with 2′,7′-dichlorofluorescin diacetate (H_2-DCFDA) in the dark (1 mg mL^{-1}, 30 min). Excess H_2-DCFDA was removed by washing with egg water, and embryos were then mounted in 1% low-gelling point agarose and carefully covered with a solution of 0.2 mg mL^{-1} tricaine to maintain anesthesia. Images were acquired using an EVOS XL Core Imaging System fitted with a GFP ($\lambda_{Ex} = 470/22$ nm, $\lambda_{Em} = 510/42$ nm) light cube.

Author Contributions

Peter J. Sadler and James P. C. Coverdale conceptualized the work. James P. C. Coverdale and Yasmin Khanom synthesized and characterized the iridium catalysts. James P. C. Coverdale performed trace elemental analysis. Millie E. Fry, Sitah A. Alsaif, Alice K. Keirle, Rebecca A. Bedford, Isolda Romero-Canelon, and James P. C. Coverdale carried out in vitro biological experiments. Millie E. Fry, Alice K. Keirle, Ji Inn Song, and James P. C. Coverdale carried out in vivo biological experiments Chloe E. Pheasey and James P. C. Coverdale carried out extracellular speciation analysis. All authors gave approval for the final version of the manuscript.

Acknowledgements

James P. C. Coverdale thanks the Royal Society of Chemistry (E22-1637945680) and the University Of Birmingham for financial support. Peter J. Sadler research is supported by Anglo American Platinum and the EPSRC (grant no. EP/P030572/1). The authors thank Dr. Abraha Habtemariam for the kind provision of Ir Cp^{xPh} and Cp^{xBip} dimer precursor compounds, and Mr. Ian Bagley for support with zebrafish in vivo studies.

Conflict of Interests

The authors declare no conflict of interest.

Data Availability Statement

The data that support the findings of this study are available in the Supporting Information of this article.

Keywords: Cancer · Catalysis · Formate · Iridium · Redox

[1] E. Panieri, M. M. Santoro, *Cell Death Dis.* **2016**, *7*, e2253–e2253.
[2] L. Chaiswing, W. H. St Clair, D. K. St Clair, *Antioxid. Redox Signal.* **2018**, *29*, 1237–1272.
[3] A. J. Sabnis, T. G. Bivona, *Trends Mol. Med.* **2019**, *25*, 185–197.
[4] a) J. J. Soldevila-Barreda, I. Romero-Canelón, A. Habtemariam, P. J. Sadler, *Nat. Commun.* **2015**, *6*, 6582; b) F. Chen, J. J. Soldevila-Barreda, I. Romero-Canelón, J. P. C. Coverdale, J.-I. Song, G. J. Clarkson, J. Kasparkova, A. Habtemariam, V. Brabec, J. A. Wolny, V. Schünemann, P. J. Sadler, *Dalton Trans.* **2018**, *47*, 7178–7189; c) F. Chen, I. Romero-Canelón, J. J. Soldevila-Barreda, J.-I. Song, J. P. C. Coverdale, G. J. Clarkson, J. Kasparkova, A. Habtemariam, M. Wills, V. Brabec, P. J. Sadler, *Organometallics* **2018**, *37*, 1555–1566; d) M. M. Haghdoost, J. Guard, G. Golbaghi, A. Castonguay, *Inorg. Chem.* **2018**, *57*, 7558–7567; e) J. J. Soldevila-Barreda, A. Habtemariam, I. Romero-Canelón, P. J. Sadler, *J. Inorg. Biochem.* **2015**, *153*, 322–333; f) A. H. Ngo, M. Ibañez, L. H. Do, *ACS Catal.* **2016**, *6*, 2637–2641; g) J. Li, L. Guo, Z. Tian, S. Zhang, Z. Xu, Y. Han, R. Li, Y. Li, Z. Liu, *Inorg. Chem.* **2018**, *57*, 13552–13563; h) D. Lovison, T. Berghausen, S. R. Thomas, J. Robson, M. Drees, C. Jandl, A. Pöthig, P. Mollik, D. P. Halter, W. Baratta, A. Casini, *ACS Catal.* **2023**, *13*, 10798–10823; i) C. Wang, J. Liu, Z. Tian, M. Tian, L. Tian, W. Zhao, Z. Liu, *Dalton Trans.* **2017**, *46*, 6870–6883; j) N. Lu, Z. Deng, J. Gao, C. Liang, H. Xia, P. Zhang, *Nat. Commun.* **2022**, *13*, 2245.
[5] a) J. P. C. Coverdale, I. Romero-Canelón, C. Sanchez-Cano, G. J. Clarkson, A. Habtemariam, M. Wills, P. J. Sadler, *Nat. Chem.* **2018**, *10*, 347–354; b) H. E. Bridgewater, E. M. Bolitho, I. Romero-Canelón, P. J. Sadler, J. P. C. Coverdale, *J. Biol. Inorg. Chem.* **2023**, *28*, 345–353.
[6] a) Z. Liu, R. J. Deeth, J. S. Butler, A. Habtemariam, M. E. Newton, P. J. Sadler, *Angew. Chem., Int. Ed.* **2013**, *52*, 4194–4197; b) E. M. Bolitho, N. G. Worby, J. P. C. Coverdale, J. A. Wolny, V. Schünemann, P. J. Sadler, *Organometallics* **2021**, *40*, 3012–3023.
[7] a) S. Banerjee, P. J. Sadler, *RSC Chem. Biol.* **2021**, *2*, 12–29; b) Z. Liu, I. Romero-Canelón, B. Qamar, J. M. Hearn, A. Habtemariam, N. P. E. Barry, A. M. Pizarro, G. J. Clarkson, P. J. Sadler, *Angew. Chem., Int. Ed.* **2014**, *53*, 3941–3946.
[8] a) J. G. Rebelein, Y. Cotelle, B. Garabedian, T. R. Ward, *ACS Catal.* **2019**, *9*, 4173–4178; b) M. Szponarski, F. Schwizer, T. R. Ward, K. Gademann, *Commun. Chem.* **2018**, *1*, 84.
[9] a) P. A. Dub, J. C. Gordon, *Dalton Trans.* **2016**, *45*, 6756–6781; b) A. M. R. Hall, D. B. G. Berry, J. N. Crossley, A. Codina, I. Clegg, J. P. Lowe, A. Buchard, U. Hintermair, *ACS Catal.* **2021**, *11*, 13649–13659.
[10] J. P. C. Coverdale, H. E. Bridgewater, J. I. Song, N. A. Smith, N. P. E. Barry, I. Bagley, P. J. Sadler, I. Romero-Canelón, *J. Med. Chem.* **2018**, *61*, 9246–9255.
[11] a) Y. Fu, C. Sanchez-Cano, R. Soni, I. Romero-Canelon, J. M. Hearn, Z. Liu, M. Wills, P. J. Sadler, *Dalton Trans.* **2016**, *45*, 8367–8378; b) J. P. C. Coverdale, R. A. Bedford, O. W. L. Carter, S. Cao, M. Wills, P. J. Sadler, *Chem. Bio. Chem.* **2024**, e202400374.
[12] H. Hao, X. Liu, X. Ge, Y. Zhao, X. Tian, T. Ren, Y. Wang, C. Zhao, Z. Liu, *J. Inorg. Biochem.* **2019**, *192*, 52–61.
[13] C. Huang, C. Liang, T. Sadhukhan, S. Banerjee, Z. Fan, T. Li, Z. Zhu, P. Zhang, K. Raghavachari, H. Huang, *Angew. Chem., Int. Ed.* **2021**, *60*, 9474–9479.
[14] K. Murata, T. Ikariya, R. Noyori, *J. Org. Chem.* **1999**, *64*, 2186–2187.
[15] J. P. C. Coverdale, C. Sanchez-Cano, G. J. Clarkson, R. Soni, M. Wills, P. J. Sadler, *Chem. Eur. J.* **2015**, *21*, 8043–8046.
[16] a) S. Cassar, I. Adatto, J. L. Freeman, J. T. Gamse, I. Iturria, C. Lawrence, A. Muriana, R. T. Peterson, S. Van Cruchten, L. I. Zon, *Chem. Res. Toxicol.* **2020**, *33*, 95–118; b) S. N. Dash, L. Patnaik, *Biol. Lett.* **2023**, *19*, 20220541; c) E. Habjan, G. K. Schouten, A. Speer, P. van Ulsen, W. Bitter, *FEMS Microbiol. Rev.* **2024**, *48*, 1–24.
[17] W.-Y. Zhang, S. Banerjee, G. M. Hughes, H. E. Bridgewater, J.-I. Song, B. G. Breeze, G. J. Clarkson, J. P. C. Coverdale, C. Sanchez-Cano, F. Ponte, E. Sicilia, P. J. Sadler, *Chem. Sci.* **2020**, *11*, 5466–5480.
[18] I. Romero-Canelón, L. Salassa, P. J. Sadler, *J. Med. Chem.* **2013**, *56*, 1291–1300.
[19] S. J. Lucas, R. M. Lord, A. M. Basri, S. J. Allison, R. M. Phillips, A. J. Blacker, P. C. McGowan, *Dalton Trans.* **2016**, *45*, 6812–6815.
[20] V. Vichai, K. Kirtikara, *Nat. Protoc.* **2006**, *1*, 1112–1116.
[21] V. Venkatesh, R. Berrocal-Martin, C. J. Wedge, I. Romero-Canelón, C. Sanchez-Cano, J. I. Song, J. P. C. Coverdale, P. Zhang, G. J. Clarkson, A. Habtemariam, S. W. Magennis, R. J. Deeth, P. J. Sadler, *Chem. Sci.* **2017**, *8*, 8271–8278.
[22] A. De Palo, D. Draca, M. G. Murrali, S. Zacchini, G. Pampaloni, S. Mijatovic, D. Maksimovic-Ivanic, F. Marchetti, *Int. J. Mol. Sci.* **2021**, 22.
[23] S. G. Lamarre, G. Morrow, L. Macmillan, M. E. Brosnan, J. T. Brosnan, *Clin. Chem. Lab. Med.* **2013**, *51*, 571–578.
[24] a) National Institute for Occupational Safety and Health, Advanced Engineering & Planning Corp, Tracor Jitco, Inc., Registry of Toxic Effects of Chemical Substances, U.S. Department of Health and Human Services, Public Health Service, Center for Disease Control, National Institute for Occupational Safety and Health, **1981**; b) W. Johnson, B. Heldreth, W. F. Bergfeld, D. V. Belsito, R. A. Hill, C. D. Klaassen, D. C. Liebler, J. G. Marks, R. C. Shank, T. J. Slaga, P. W. Snyder, F. A. Andersen, *Int. J. Toxicol.* **2016**, *35*, 41S–54S.
[25] a) X. M. He, D. C. Carter, *Nature* **1992**, *358*, 209–215; b) S. Sugio, A. Kashima, S. Mochizuki, M. Noda, K. Kobayashi, *Protein Eng. Des. Sel.* **1999**, *12*, 439–446.
[26] W. Bal, J. Christodoulou, P. J. Sadler, A. Tucker, *J. Inorg. Biochem.* **1998**, *70*, 33–39.
[27] S. Tayyab, S. R. Feroz, in Advances in Protein Chemistry and Structural Biology (Ed: R. Donev), Vol. *123*, Academic Press, **2021**, pp. 193–218.
[28] a) M. H. M. Klose, A. Schöberl, P. Heffeter, W. Berger, C. G. Hartinger, G. Koellensperger, S. M. Meier-Menches, B. K. Keppler, *Monatsh. Chemie.* **2018**, *149*, 1719–1726; b) J. Wang, J. Tao, S. Jia, M. Wang, H. Jiang, Z. Du, *Pharmaceuticals* **2021**, *14*, 104; c) S. A. Kozieł, M. K. Lesiów, D. Wojtala, E. Dyguda-Kazimierowicz, D. Bieńko, U. K. Komarnicka, *Pharmaceuticals* **2021**, *14*, 685; d) N. Cetinbas, M. I. Webb, J. A. Dubland, C. J. Walsby, *J. Biol. Inorg. Chem.* **2010**, *15*, 131–145; e) V. Novohradský, A. Bergamo, M. Cocchietto, J. Zajac, V. Brabec, G. Mestroni, G. Sava, *Dalton Trans.* **2015**, *44*, 1905–1913.
[29] a) F. Chiodi, Å. Sidén, E. Ösby, *Electrophoresis* **1985**, *6*, 124–128; b) A. B. Edmundson, M. Schiffer, K. R. Ely, M. K. Wood, in *Progress in Molecular and Subcellular Biology* (Ed: F. E. Hahn), Vol. *3*, Springer, Berlin, Heidelberg, **1973**, pp. 159–182.
[30] K. Marković, R. Milačič, S. Marković, J. Kladnik, I. Turel, J. Ščančar, *Molecules* **2020**, *25*, 1512.
[31] A. Managò, K. A. Becker, A. Carpinteiro, B. Wilker, M. Soddemann, A. P. Seitz, M. J. Edwards, H. Grassmé, I. Szabò, E. Gulbins, *Antioxid. Redox Signal.* **2015**, *22*, 1097–1110.
[32] J. Tönnemann, J. Risse, Z. Grote, R. Scopelliti, K. Severin, *Eur. J. Inorg. Chem.* **2013**, *2013*, 4558–4562.
[33] P. L. Olive, J. P. Banáth, *Nat. Protoc.* **2006**, *1*, 23–29.

Manuscript received: August 28, 2024
Revised manuscript received: October 03, 2024
Accepted manuscript online: October 04, 2024
Version of record online: ■■, ■■